Arab Journal of Nuclear Science and Applications, 48(4), (159-169) 2015

Frequency-Based Pulse Shape Analysis for Optimal Digitization and Discrimination

H. I. Saleh
Radiation Engineering Department, National Center for Radiation Research and Technology (NCRRT), Atomic Energy Authority, Nasr City, Cairo, Egypt.

Received: 2/3/2015 **Accepted: 5/5/015**

ABSTRACT

This paper introduces a mathematical analysis of scintillation pulses based on their frequency magnitude squares spectrum in order to determine the most discriminated frequency band of two different pulse-types spectrums. The proposed analysis showed that the most discriminated frequency band depends on the two decay-constant values of the pulse-types. Based on this analysis, a digitization criterion is proposed to determine the optimum sampling rate, number of used samples and the anti-aliasing filtering requirements. Therefore, the sampling rate, the number of samples and the cutoff of the anti-aliasing filter can be optimally selected to reduce the discrimination complexity. Moreover, determining the most discriminated frequency band reduces the number of needed frequency components and provides the highest discrimination performance with the lowest number of required computations. The proposed digitization criterion is applied on two pulse-types with different decay-time constants (τ_1 = 20 and τ_2 = 40 ns) and shows that the most discriminated frequency component is 5.627 MHz and one of optimum digitization selections is sampling rate of 24 MHz, 8-samples, and anti-aliasing filter with 8 MHz cutoff frequency.

Key words: Pulse Shape Analysis, PSD, Depth of Interaction, PET

INTRODUCTION

Scintillators are commonly used in gamma and neutron spectroscopy [1, 2], particle identification [3], and radiation therapy and diagnosis instrumentation such as gamma cameras [4,5] and Positron Emission Tomography (PET) scanners[6]. Scintillation detectors usually consist of crystals optically coupled to photomultiplier tubes (PMTs). The scintillation crystal responds to the absorption of the incident radiation by the emission of a light pulse which is characterized by the special properties of the crystal such as the decay time constant [1]. Then, the PMT generates an electrical pulse relative to the absorbed radiation energy.

The decay time constant of the pulse varies with the type of incident particle enabling pulse shape discrimination (PSD), i.e., particle identification. Thus, based on the decay characteristics of the electric pulse, the γ rays and α particles can be identified based on the decay time of the PMT signal [7]. Similarly, the falling portions of a neutron pulse and a γ-ray pulse are significantly different and can be identified based on the decay time of their pulses [8]. On the other hand, a stack of two or more different scintillation crystals optically coupled to a single PMT (called a phoswich detector) is used in PET systems in order to reduce the Depth of Interaction (DOI) error[9]. Thus, the crystal identification (CI) requires applying pulse shape discrimination (PSD) methods[10] to identify the scintillated crystal according to decay time constant of its pulse.

In Digital PSD, the output of detector or preamplifier is digitized and sampled data are transferred to computer memory from an onboard memory for future analysis. Digital PSD methods provide more flexibility than conventional methods in handling individual pulses and performing pulse shape analysis. The advantages of digital methods are reduced hardware, increased flexibility,

improved performance, throughput rate etc. These PSD methods can be classified into time-domain and frequency-domain.

Compared with time domain, the methods developed in frequency domain are more robust to the natural variance in the pulse response arising from the PMT. Therefore, the Fast Fourier Transform (FFT) of the pulses improved the CI performance[11]. Moreover, the normalized last sample (NLS) method[12], which is dependent strongly on one sample, reduces the FFT complexity at the expense of performance. Other researchers suggested a discrete wavelet (DWT) decomposition of the pulses as an alternative[13,14,15,16] to obtain a moderate complexity and a good performance. Also, the discrete cosine transforms (DCT) [17] were presented as CI methods. Different classifiers such as the cross fuzzy logic[18], neural network[19], correlation and the principle component analysis (PCA)[20] were employed in the PSD and CI methods.

Recently, the two-dimensional Zernike moments (2D-ZMs) were applied to identify the scintillating crystal type[21]. In this approach, the ZMs vector represents the extracted features of the pulse and is classified by the Euclidean distance. The 2D-ZM CI method has the highest identification performance among other recent methods but it is too complex to fulfill the real time requirements of PET scanners[21]. A 1-D form of the ZMs was proposed to simplify the computational complexity of ZMs for the 1-D pulses which are classified by the support vector machine (SVM) to gain the same 2D-ZM CI performance. Using one pre-calculated vector of support vector coefficients, the cascaded ZMs and SVM are combined into one multiplier-accumulator to obtain one vector of pre-calculated coefficients. Thus, the 1-D ZM-SVM CI method has an increased performance and a reduced complexity to comply with the real time rate of PET[22].

To the best of the knowledge of the author, there is no method in the literature addressing how to select the sampling rate of the pulse digitization, the number of samples, and the most discriminated frequency components. The aim of the present work is to introduce a mathematical analysis of the pulses in order to determine the most discriminated frequency band. The proposed analysis showed that the most discriminated frequency band depends on the two decay-constant values of the pulse-types. Based on this analysis, a digitization criterion is proposed to determine the optimum sampling rate, the number of used samples and the anti-aliasing filtering requirements in order to reduce the discrimination complexity. This new method will assist the PSD system designers in selecting the optimal digitization parameters; i.e. the sampling rate, the number of samples and the most discriminated frequency component. The use of these optimal digitization parameters reduces the number of needed frequency components and provides the highest discrimination performance with the lowest number of required computations.

The following section II introduces the proposed analysis method. The proposed digitization criterion for optimal selection of the sampling rate, number of samples and the most discriminated frequency component is presented in Section III. The proposed method is applied on two different pulse-types and their results are showed and discussed in Section IV. Finally, the conclusion is provided in Section V.

PULSE SHAPE ANALYSIS METHOD

The proposed analysis uses the frequency spectrum of the pulses to discriminate between two pulse-types with different decay-time constants. The pulse can be simply expressed as a single sided exponential pulse as follows:

$$p = ae^{-t/\tau}, \qquad (1)$$

Where a and τ are the peak and the decay-time constant of the pulse, respectively.

Using the Continuous Time Fourier Transform (CTFT), the Frequency spectrum of the pulse is given by

$$P = \frac{a}{\frac{1}{\tau}+j\omega} \qquad (2)$$

The magnitude square of the Fourier spectrum is

$$|P|^2 = \frac{a^2}{\frac{1}{\tau^2}+\omega^2} \qquad (3)$$

The normalized magnitude square of the Fourier spectrum is

$$NF = \frac{|P(\omega)|^2}{|P(0)|^2} = \frac{1}{1+\omega^2\tau^2} \qquad (4)$$

For two different pulse-types, p_1 and p_2, where $p_1$has a shorter decay time τ_1 than that of p_2 (τ_2), the normalized frequency magnitude squares difference; i.e. normalized with respect to zero frequency component square, ($NF_1 - NF_2$) is given by

$$\text{diff}=NF_1 - NF_2 = \frac{1}{1+\omega^2\tau_1^2} - \frac{1}{1+\omega^2\tau_2^2} \qquad (5)$$

The maximum difference between the magnitudes squares of the normalized spectrums occurs at

$$\omega_{\max} = \frac{1}{(\tau_1\tau_2)^{0.5}} \qquad (6)$$

which is computed by equating $\frac{\mathrm{d}(\text{diff})}{\mathrm{d}\omega}$ to zero. Thus, the maximum difference is given by:

$$\text{diff}_{\max} = \frac{\tau_2-\tau_1}{(\tau_2+\tau_1)} \qquad (7)$$

The effects of using a finite sampling rate ($1/T_s$) and a finite number of samples (L) on the frequency spectrum of the digitized pulse $p_{(nT_s)} = a\,e^{-nT_s/\tau}$ can be introduced by computing the Discrete-Time Fourier Transform (DTFT) as:

$$\hat{P}_L(f) = \sum_{n=0}^{L} \left(e^{-\frac{T_s}{\tau}} e^{-2\pi j f T_s}\right)^n \qquad (8)$$

By applying the Euler's finite summing series

$$\sum_{n=0}^{L} x^n = \frac{1-x^L}{1-x} \qquad (9)$$

One can get the normalized magnitude square of the spectrum as follows:

$$N\hat{F}_L = \frac{\left|\hat{P}_L(f)\right|^2}{\left|\hat{P}_L(0)\right|^2} = \frac{(1-2e^{-T_sL/\tau}\cos(2\pi f T_s L)+e^{-2T_sL/\tau})}{(1-2e^{-T_s/\tau}\cos(2\pi f T_s)+e^{-2T_s/\tau})}\frac{(1-e^{-T_s/\tau})^2}{(1-e^{-T_sL/\tau})^2} \qquad (10)$$

For infinite number of samples (L → ∞), the normalized squared magnitude of the spectrum tends to

$$N\hat{F} = \frac{(1 - e^{-T_s/\tau})^2}{(1 - 2e^{-T_s/\tau}\cos(2\pi f T_s) + e^{-2T_s/\tau})} \qquad (11)$$

The normalized squared magnitude of the spectrum of pulse $p_{1(nT_s)}$ is given by:

$$N\hat{F}_1 = \frac{\left|\hat{P}_1(f)\right|^2}{\left|\hat{P}_1(0)\right|^2} = \frac{(1 - e^{-T_s/\tau_1})^2}{(1 - 2e^{-T_s/\tau_1}\cos(2\pi f T_s) + e^{-2T_s/\tau_1})} \qquad (12)$$

Similarly, for the second pulse type

$$N\hat{F}_2 = \frac{\left|\hat{P}_2(f)\right|^2}{\left|\hat{P}_2(0)\right|^2} = \frac{(1 - e^{-T_s/\tau_2})^2}{(1 - 2e^{-T_s/\tau_2}\cos(2\pi f T_s) + e^{-2T_s/\tau_2})} \qquad (13)$$

The difference between the magnitude squares of the normalized spectrums of two different types is:

$$D = N\hat{F}_1 - N\hat{F}_2 = \frac{\left(1 - e^{-\frac{T_s}{\tau_1}}\right)^2}{\left(1 - 2e^{-\frac{T_s}{\tau_1}}\cos(2\pi f T_s) + e^{-\frac{2T_s}{\tau_1}}\right)} - \frac{\left(1 - e^{-\frac{T_s}{\tau_2}}\right)^2}{\left(1 - 2e^{-\frac{T_s}{\tau_2}}\cos(2\pi f T_s) + e^{-\frac{2T_s}{\tau_2}}\right)} \qquad (14)$$

Similarly, the difference between the normalized magnitude squares of two different types using L samples is:

$$D_L = N\hat{F}_{L1} - N\hat{F}_{L2} =$$

$$\frac{(1 - 2e^{-T_s L/\tau_1}\cos(2\pi f T_s L) + e^{-2T_s L/\tau_1})}{(1 - 2e^{-T_s/\tau_1}\cos(2\pi f T_s) + e^{-2T_s/\tau_1})}\frac{(1 - e^{-T_s/\tau_1})^2}{(1 - e^{-T_s L/\tau_1})^2} - \frac{(1 - 2e^{-T_s L/\tau_2}\cos(2\pi f T_s L) + e^{-2T_s L/\tau_2})}{(1 - 2e^{-T_s/\tau_2}\cos(2\pi f T_s) + e^{-2T_s/\tau_2})}\frac{(1 - e^{-T_s/\tau_2})^2}{(1 - e^{-T_s L/\tau_2})^2} \qquad (15)$$

THE PROPOSED DIGITIZATION CRITERION

According to the Nyquist theorem, within the central Nyquist interval [$\frac{-f_s}{2}, \frac{f_s}{2}$], the two spectra $N\hat{F}$ and NF agree approximately, especially at low frequencies. This approximation gets better as f_s increases; i.e. T_s decreases. However, outside these intervals, the sampled spectra repeat periodically. Therefore, the sampling frequency f_s should be selected to assure that:

$$\frac{f_s}{2} > f_{max} = \frac{1}{2\pi(\tau_1\tau_2)^{0.5}}$$

i.e.

$$f_s = Bf_{max} = B\frac{\sqrt{r}}{2\pi\tau_1} \qquad (16)$$

Where the factor $B > 2$.

Since, $0 < \sqrt{r} < 1 \ for\ 0 < \frac{\tau_1}{\tau_2} < 1$, the sampling frequency $f_s = \frac{1}{\tau_1}$ satisfies the above condition for any practical value of the decay-times ratio ($r = \frac{\tau_1}{\tau_2}$).

The n[th] frequency component of the Discrete Fourier Transform (DFT) is given by:

$f_n = n/LT_s, where$ the frequency component index $n = 0,1, \ldots, L-1$. (17)

Substitute from (17) in (10) and (15)

The normalized magnitude square of the spectrum component is as follows:

$$N\hat{F}_L(n) = \left|N\hat{P}_L(n)\right|^2 = \frac{(1 - 2e^{-T_sL/\tau}\cos(2\pi n) + e^{-2T_sL/\tau})}{(1 - 2e^{-T_s/\tau}\cos(2\pi n/L) + e^{-2T_s/\tau})}\frac{(1 - e^{-T_s/\tau})^2}{(1 - e^{-T_sL/\tau})^2}$$

$$= \frac{(1 - e^{-T_s/\tau})^2}{(1 - 2e^{-T_s/\tau}\cos(2\pi n/L) + e^{-2T_s/\tau})} \qquad (18)$$

The difference between the magnitudes squares of the normalized components of two different types is:

$$D_L(n) = \frac{(1 - e^{-T_s/\tau_1})^2}{(1 - 2e^{-T_s/\tau_1}\cos(2\pi n/L) + e^{-2T_s/\tau_1})} - \frac{(1 - e^{-T_s/\tau_2})^2}{(1 - 2e^{-T_s/\tau_2}\cos(2\pi n/L) + e^{-2T_s/\tau_2})} \qquad (19)$$

In order to gain the maximum difference of frequency magnitudes, one of the frequency components (except the DC component) must be adjusted to be in coherent with the value of f_{max} (i.e. the most discriminated frequency component). Since, the (n+1)[th] frequency component of the DFT is computed as follows:

$$f_{n+1} = \frac{nf_s}{L} = f_{max} \qquad (20)$$

From equations (16) and (20), we get

$$L = nB \qquad (21)$$

Where $n = 1,2,..,L/2$ and $B > 2$

From (21), equation (16) can be rewritten as

$$f_s = \frac{L}{n}f_{max} \qquad (22)$$

Therefore, the digitization criterion of f_s and L can be stated in the following manner:

Firstly, compute the f_{max} according to equation (6), secondly select $L \geq 2$, finally select f_s according to equation (16)

Another condition for selecting f_s and L is the sampling time window, i.e. $LT_s \geq 4\tau_1$ (23).

RESULTS AND DISCUSSIONS

In order to show how to define the optimal sampling rate and number of samples used in the PSD of two different pulses types, the digitization criterion is applied on two pulses $p_1$and p_2 with decay-time constants τ_1 =20 and $\tau_2 = 40$ ns, respectively. Using equation (4), the normalized spectrums of magnitude squares of both pulse-types and their difference given by equation (5) are calculated and plotted in Fig. (**1**).

Fig. (**1**) shows the CTFT of the two pulse-types and their spectra difference indicating the frequency f_{max} where the maximum difference obtained. From Fig. **(1**, f_{max} equals 5.627 MHz which complies with the value computed from equation (6) for $\tau_1 = 20\,ns$ and $\tau_2 = 40\,ns$. By selecting the sampling frequency according to the proposed digitization criterion, f_s is greater than $2f_{max}$. For simplicity, f_s is taken equal to 12 MHz or its multiples to study the oversampling effects on the spectrum replicas.

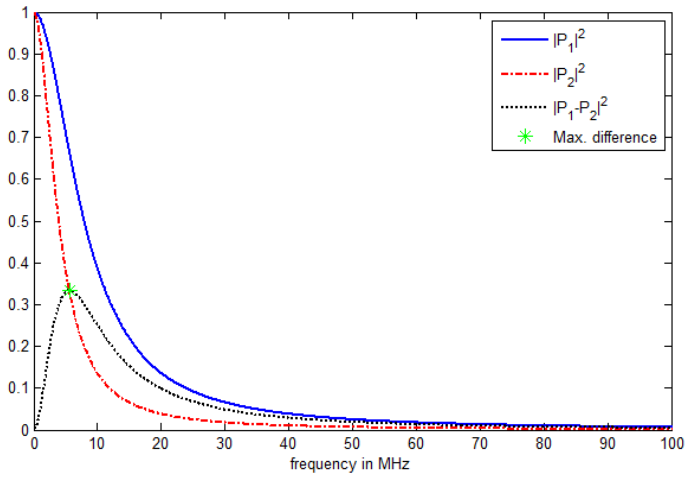

Fig. (1): Frequency magnitudes squares spectrums of P_1 ($\tau_1 = 20\,ns$) and P_2 ($\tau_2 = 40\,ns$), and their differences indicating the maximum difference of spectrums at 5.627 MHz.

Using different sampling rates of 12, 24, 48, and 96 MHz, the normalized spectra of magnitude squares of the first ($\tau_1 = 20\,ns$) and second ($\tau_2 = 40\,ns$) pulse-types, are shown in Figure 2 and Figure 3, respectively. In Figure 2 and Figure 3, the CTFT, DTFT, DTFT using 8-samples window, and DFT using 8-samples window are calculated from equations (4), (12), (10) and (18) respectively.

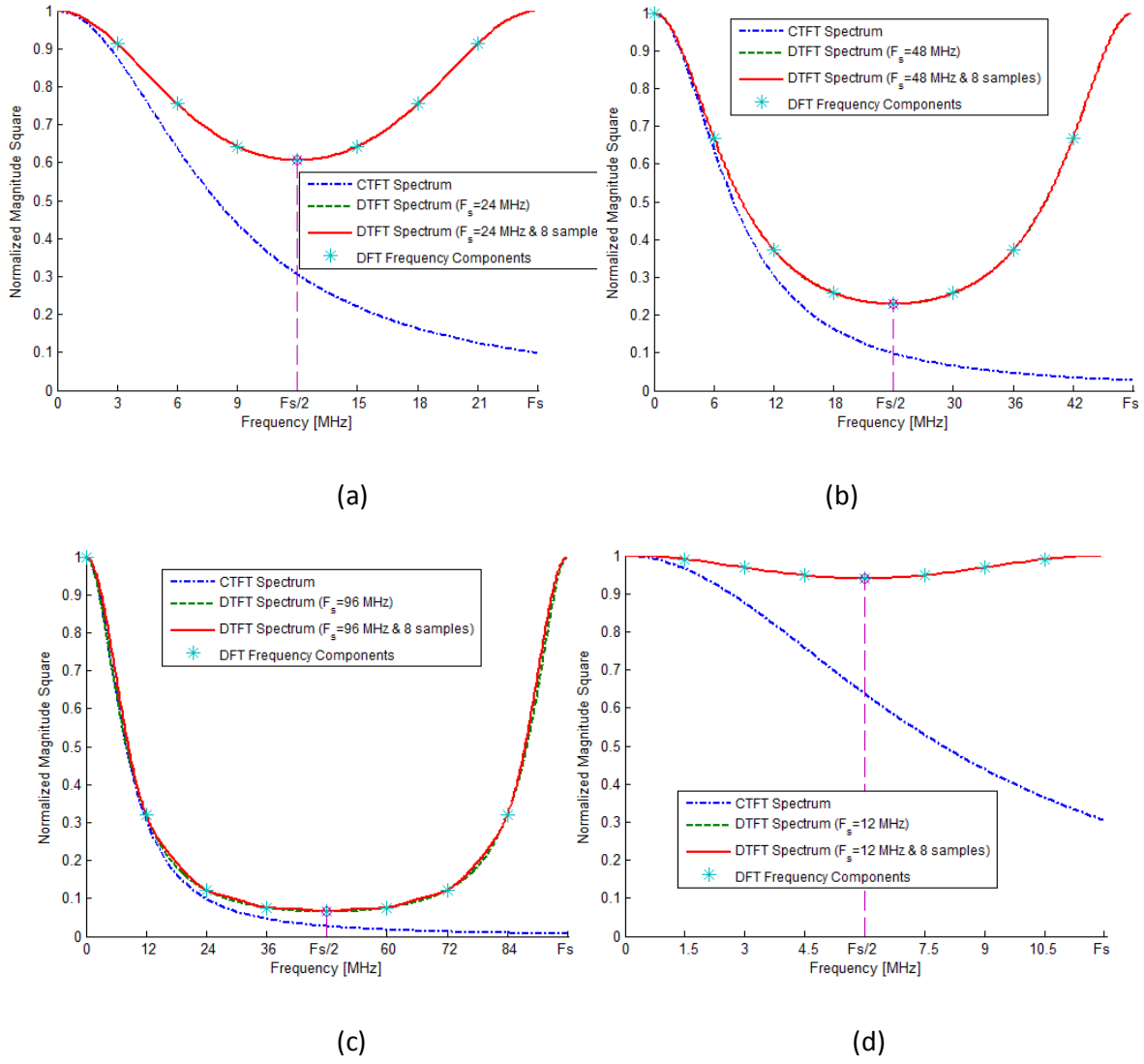

Fig. (2): Normalized spectra of frequency magnitudes squares for P_1 ($\tau_1 = 20\,ns$) using different Fourier transforms at sampling rates of (a) 24, (b) 48, (c) 96, and (d) 12 MHz; for a window of 8 samples.

Figure 2(a) presents the normalized spectra of magnitude squares of the first pulse-type using different Fourier transforms with sampling rate of 24 MHz. However, the Figures 2(b), 2(c) and 2(d) are obtained using sampling rates of 48, 96, 12 MHz. The DTFT spectra approximately agree with the original analogue spectrum (CTFT) at low frequencies while by reaching the Nyquist frequency (f_s/2), the DTFT spectra and the CTFT are different from each other. By increasing the sampling rate, the DTFT spectra become closer to the CTFT spectrum, see Figure 2 (c) which has sampling rate of 96 MHz compared with Figure 2 (d) with sampling rate of 12 MHz.

Similarly, Figure 3 shows the effects of the different sampling rates on the DTFT spectra for the second pulse type p_2 and how they approach the original CTFT spectrum.

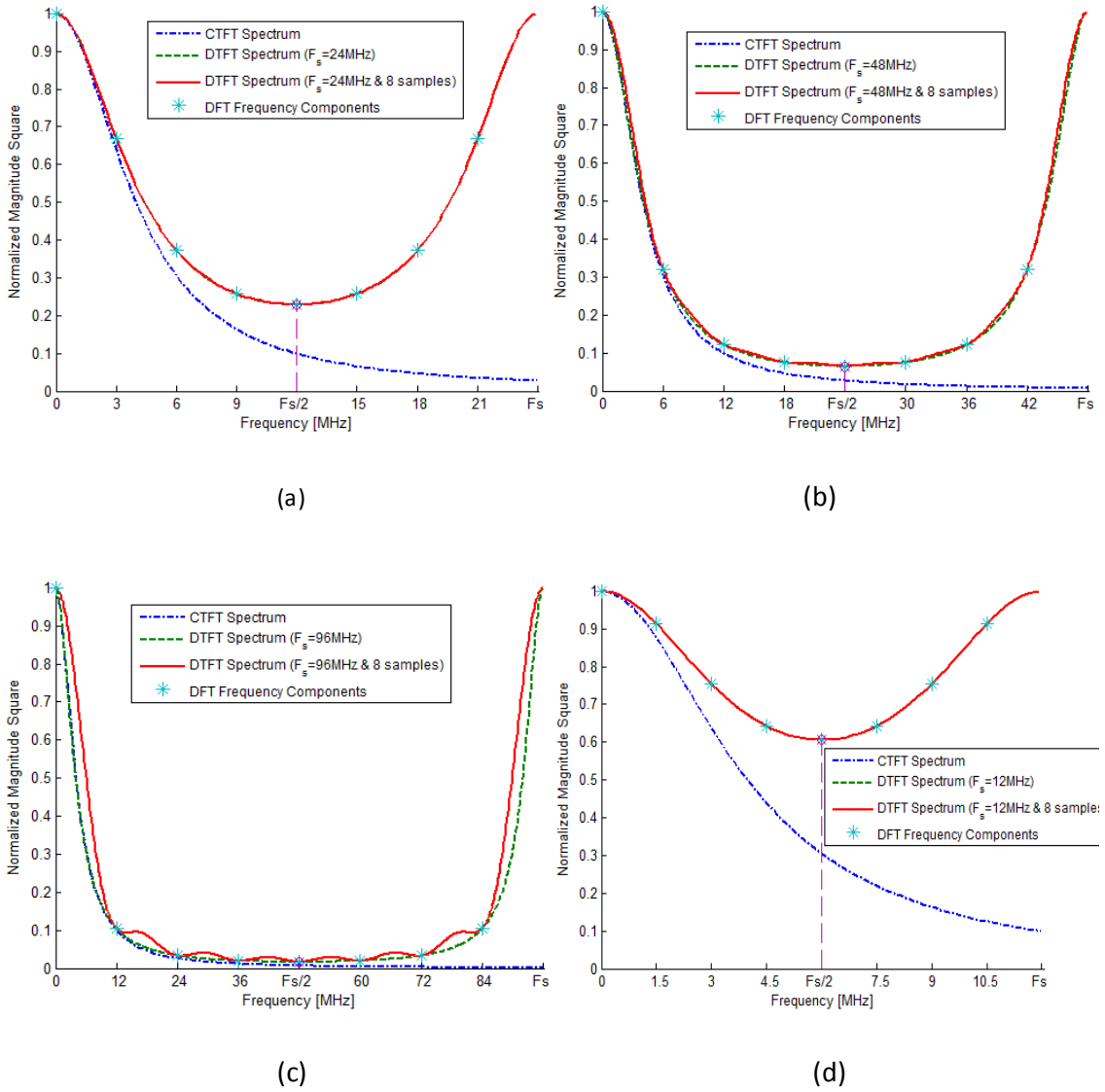

Fig. (3): Normalized Spectra of frequency magnitudes squares for p_2 ($\tau_2 = 40\ ns$)using different Fourier transforms at sampling rates of (a) 24, (b) 48, (c) 96, and (d) 12 MHz; for a window of 8 samples.

Fig. (4: Shows the differences of the normalized spectra of magnitude squares of the first ($\tau_1 = 20\ ns$) and second ($\tau_2 = 40\ ns$) pulse-types using sampling rates of 24, 48, 96, and 12 MHz.

From Figure 4(b) and 4(c), the oversampling can be used to reduce the attenuation requirements by the anti-aliasing filter and thus its order. Moreover, using higher multiples of sampling rates reduces aliasing and allows less sharp cutoffs for the anti-aliasing filter.

Using 8 samples to represent the DFT spectrum with sampling rate of 12 MHz, see Figure 4(d), puts the 5th frequency component on 6 MHz (i.e. the Nyquist frequency; $\frac{f_s}{2}$) which has the maximum difference of spectra, but the anti-aliasing filter dramatically attenuates this component to reduce the aliasing effects. By using the double of this sampling rate; i.e. 24 MHz, and 8-samples window of the pulses, the anti-aliasing filter should have a cutoff greater than 6 MHz and a sharp transition band. Thus, as shown in **Fig. (4** (a), the third DFT component has the maximum difference of the two spectra which complies with the given method as in equation (20) for n=2, L=8.

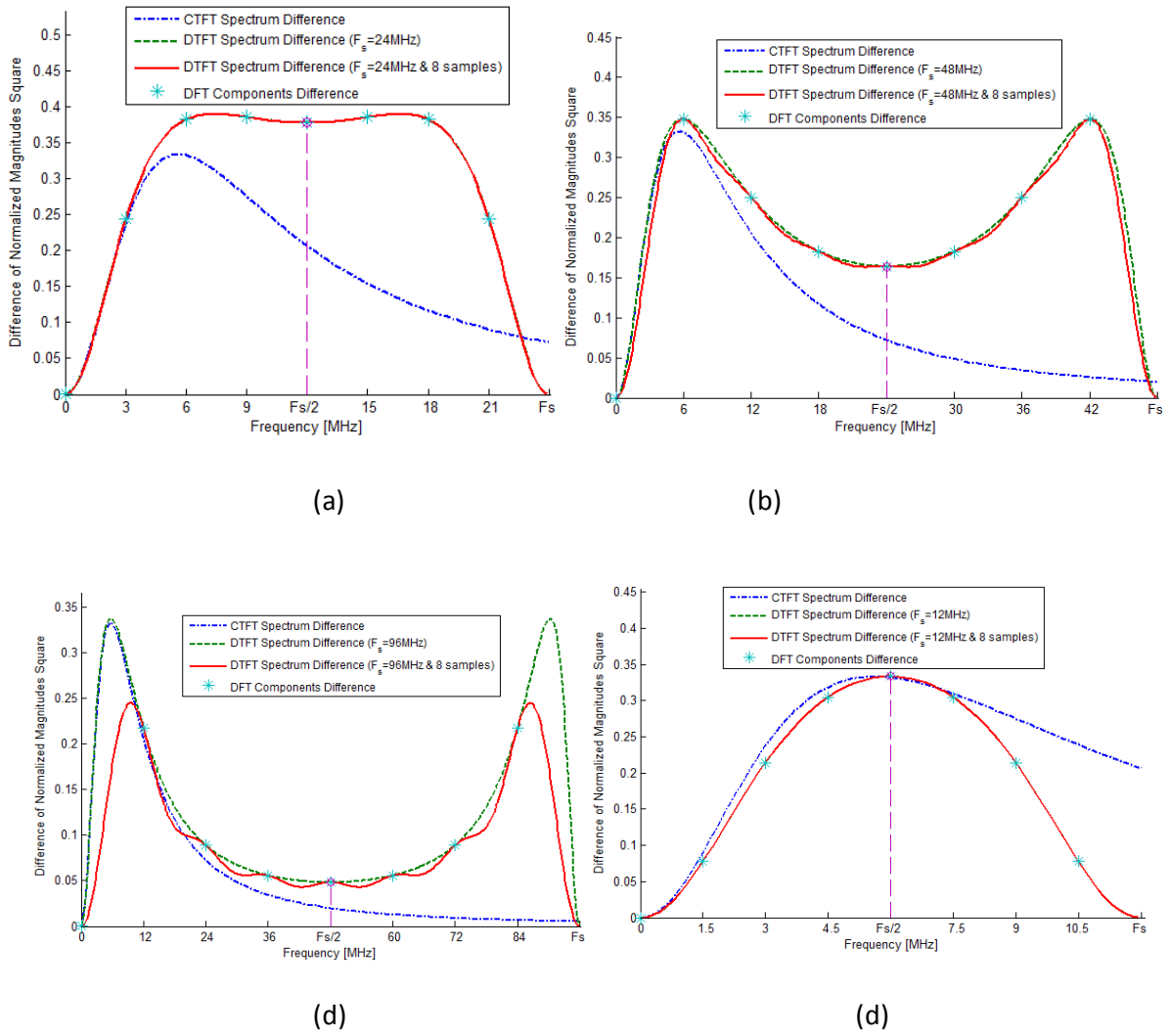

Fig. (4): Normalized differences of frequency magnitudes squares spectra using different fourier transforms at sampling rates of (a) 24, (b) 48, (c) 96, and (d) 12 MHz; for a window of 8 Samples.

The effects of using band-limited pulses; i.e. finite number of samples, are shown in Figures 2 and 3, where 8-samples are used to represent the DTFT and DFT with different sampling rates of 12, 24, 48, and 96 MHz. For 96 MHz sampling rate ($T_S \approx 10.4$ ns), the DTFT using 8-samples has a Sinc function modulation effect, as shown in **Fig. (3**(c), due to using a limited rectangular window of time; the $LT_S \approx 83.2$ ns which is less than $4\,\tau_2$ as mentioned in equation (23). Therefore, in order to reduce the effects of the limited rectangular window of time on the frequency spectrum of the pulse p_2, the time-window; i.e. LT_S, should be greater than $4\,\tau_2$.

Two different data sets of phoswich detectors were treated in references[16,17,21,22]. The first data set of two pulse-types (LSO and LuYAP) with 40 ns, and 220 ns decay-time constants, respectively. On the other hand, the second data set has two pulse-types with 40 ns, and 60 ns decay-time constants. Both data sets were anti-aliased filtered with cutoff 3MHz, and digitized into 16 samples (i.e. time window of 400 ns) with sampling rate of 40 MHz. By applying our analysis method, the most discriminated frequency component f_{max} is 1.696 MHz and 3.248 MHz for the first and second data sets, respectively. Hence, the anti-aliasing filter attenuated the most discriminated frequency

component of the second data set while preserved it in the first data set. Therefore, the first data set has a higher discrimination performance (99%)[17] than that of the second type data set (92%)[21]. Moreover, using 16 samples gives a DFT frequency resolution of 2.5 MHz which implies that the second DFT component is the most discriminated one in both data sets.

Based on our digitization criterion, one can recommend using an anti-aliasing filter with 5 MHz cutoff frequency, a sampling rate of 16 MHz, and 10 samples in order to get the DFT components at 1.6 MHz, and 3.2 MHz and to simplify the filtering requirements and computations of the discrimination system.

CONCLUSION

A mathematical analysis based on the frequency magnitude squares spectrum of two different types of scintillation pulses has been introduced in order to determine the most discriminated frequency band. It has been shown that the most discriminated frequency band depends on the two decay-constant values of the pulse-types. Moreover, the most discriminated frequency component is given by a derived mathematical equation. Based on this analysis, a digitization criterion is proposed to determine the optimum sampling rate, number of used samples and the anti-aliasing filtering requirements in order to reduce the discrimination system complexity. To prove the effectiveness of the proposed digitization criterion, it was applied on two pulse-types with decay constants of 20 and 40 ns. The results showed that, the advised anti-aliasing filter has an 8 MHz cutoff and the optimum sampling rate is 24 MHz using 8 input samples to get the maximum difference of spectra at the third component; i.e. 6 MHz. This compromised selection requires a moderate rate of sampling in addition to simple anti-aliasing filter requirements. The discrimination results of two recently-processed data sets of scintillation pulses have been studied in light of our digitization criterion which recommended using a sampling rate of 16 MHz, 10 samples and an anti-aliasing filter with 5 MHz cutoff frequency instead of the used 3 MHz, in order to obtain a higher discrimination rate. This study provides the framework for a new way to determine the optimum sampling rate, number of used samples and the anti-aliasing filtering requirements in order to reduce the complexity of and increase the rate of the discrimination systems.

REFERENCES

(1) G.F. Knoll, Radiation Detection and Measurement, John Wiley & Sons, New York, 1999.

(2) Guofu Liu, Malcolm J. Joyce, Xiandong Ma, and Michael D. Aspinall, “A Digital Method for the Discrimination of Neutrons and γ Rays With Organic Scintillation Detectors Using Frequency Gradient Analysis,” IEEE Trans. Nucl. Sci., vol. 57, no. 3, pp. 1682–1691, June 2010.

(3) M. Faisal, R.T. Schiffer, M. J. Haling, M. Flaska, S. A. Pozzi, and D. D. Wentzloff, “A Data Processing System for Real-Time Pulse Processing and Timing Enhancement for Nuclear Particle Detection Systems,” IEEE Trans. Nucl. Sci., vol. 60, no. 2, pp. 619–623, April 2013.

(4) R. Britton, J. L. Burnett, A. V. Davies, and P. H. Regan, "Coincidence corrections for a multi-detector gamma spectrometer," Nuclear Instruments and Methods in Physics Research Section A: Accelerators, Spectrometers, Detectors and Associated Equipment, vol. 769, pp. 20-25, 2015.

(5) J. H. Lee, H. S. Jung, H. Y. Cho, Y. K. Kwon, and C. S. Lee, “A Novel Digital Pulse-Shape Analysis for High-Resolution Position-Sensitive Gamma-Ray Spectroscopy,” IEEE Trans. Nucl. Sci., vol. 57, no. 5, pp. 2631–2637, Oct. 2010.

(6) L. Eriksson, C. L. Melcher, M. Eriksson, H. Rothfuss, R. Grazioso, and M. Aykac, "Design Considerations of Phoswich Detectors for High Resolution Positron Emission Tomography," IEEE Transactions on Nuclear Science, vol. 56, pp. 182-188, 2009.

(7) H. Bagan, A. Tarancon, G. Rauret, and J. F. Garcia, "Alpha/beta pulse shape discrimination in plastic scintillation using commercial scintillation detectors," Anal Chim Acta, vol. 670, pp. 11-7, Jun 2010.

(8) G. H. V. Bertrand, M. Hamel, S. Normand, and F. Sguerra, "Pulse shape discrimination between (fast or thermal) neutrons and gamma rays with plastic scintillators: State of the art," Nuclear Instruments and Methods in Physics Research Section A: Accelerators, Spectrometers, Detectors and Associated Equipment, vol. 776, pp. 114-128, 2015.

(9) Soriano, Antonio, et al. "Minimization of parallax error in dedicated breast PET." Nuclear Science, IEEE Transactions on vol. 60, no. 2, pp. 739-745, April 2013.

(10) A. P. I. Siddavatam, "METHODS OF PULSE SHAPE DISCRIMINATION (PSD)," VESIT, International Technological Conference-2014 (I-TechCON), Jan. 03 – 04, 2014, pp. 281-284.

(11) H. Saleh, E. Zimmermann, and H. Halling, "Method For Assigning A Pulse Response To One Of A Plurality Of Pulse Types With Different Decay Times And Device For Carrying Out Said Method", Patents, Apr. 10, 2007, US 7202479.

(12) M. Streun, G. Brandenburg, H. Larue, H. Saleh, E. Zimmermann, K. Ziemons, and H. Halling, "Pulse Shape Discrimination of LSO and LuYAP Scintillators for Depth of Interaction Detection in PET", IEEE Transaction on Nuclear Science, vol. 50, no. 3, June 2003.

(13) S. Yousefi, L. Lucchese, "A wavelet-based pulse shape discrimination method for simultaneous beta and gamma spectroscopy", Nuclear Instruments and Methods in Physics Research Section A, vol. 599, pp. 66–73, 2009.

(14) H. Semmaoui, N. Viscogliosi, R. Fontaine, R. Lecomte, "Wavelets-Based Crystal Identification of Phoswich Detectors for Small-Animal PET". IEEE Transactions on Nuclear Science, vol. 55, no. 3, June 2008.

(15) A. Arafa, H. Saleh, M. Ashour, A. Salem, "Investigation of Different Wavelets for Pulse Shape Discrimination of LSO and LuYAP Scintillators in Positron Emission Tomography", Computer Engineering & Systems International Conference, ICCES2009, p.p. 610 – 615, 14-16 December, 2009.

(16) A. A. Arafa, H. I. Saleh, M. Ashour, and A. Salem, "FFT- and DWT-based FPGA realization of pulse shape discrimination in PET system," in Design & Technology of Integrated Systems in Nanoscal Era, 2009. DTIS '09. 4th International Conference on, 2009, pp. 299-302.

(17) H. Saleh, A. Yahya, M. Ashour, and M. Sayed, "DST and DCT-based Depth of Interaction (DOI) Determining Techniques for LSO and LuYAP Scintillation Detectors in PET," *International Journal of Computer Applications*, vol. 28, pp. 41-45, 2011.

(18) S. Yousefi, L. Lucchese, "Digital Pulse Shape Discrimination in Triple-Layer Phoswich Detectors Using Fuzzy Logic", IEEE Transactions On Nuclear Science, Vol. 55, No. 5, October 2008.

(19) P. Guazzoni, F. Previdi, S. Russo, M. Sassi, S.M. Savaresi, L. Zetta, "Pulse shape analysis using subspace identification methods and particle identification using neural networks in CsI(Tl) scintillators", IEEE Nuclear Science Symposium Conference Record, Vol. 3, pp. 1341-1345, 23-29 October 2005.

(20) H. Saleh, A. Yahya, M. Sayed, and M. Ashour, "Pulse Shape Discrimination Techniques Based on Cross-Correlation and Principal Component Analysis," *International Journal of Computer Applications*, vol. 38, pp. 6-11, 2012.

(21) A. A. Arafa, H. I. Saleh, and M. A. Ashour, "A zernike moment method for pulse shape discrimination in PMT-based PET detectors," IEEE Trans. Nucl. Sci., vol. 60, no. 3, pp. 1518–1526, Jun. 2013.

(22) A. A. Arafa, and H. I. Saleh, "A Real-Time Scintillation Crystal Identification Method and Its FPGA Implementation," IEEE Trans. Nucl. Sci., vol. 61, no. 5, pp. 2439–2445, Oct. 2014.